HiSST: 3rd International Conference on
High-Speed Vehicle Science Technology
14 -19 April 2024, Busan, Korea

High Fidelity Simulation of Liquid Jet Breakup in Supersonic Crossflow

Donggyu Yun[1], Hong-Gye Sung[2]

Abstract

The liquid break-up and spray combustion in supersonic crossflow are primarily encountered in scramjet engines. An angled liquid jet injector can be considered as the effective way enhancing the liquid break-up and atomize in certain time. The process of liquid fuel atomization and mixing of fuel injection involves multiple complex phenomena that are closely interconnected. This study aims to provide a comprehensive simulation of the processes of ligament and droplet breakup and atomization in an angled jet in supersonic crossflow using the homogeneous mixture model (HMM) and large eddy simulation (LES). Furthermore, numerical techniques are applied, including the Novel-Abel Stiffened Gas (NASG) state equation, Adaptive Mesh Refinement (AMR), Synthetic Eddy Method (SEM), and the Eulerian-Lagrangian (EtoL) transformation. The complex structures, such as shockwaves and vortices such as the bow shock, horseshoe vortex, and counter-rotating vortex pair, around the liquid column are investigated. Without using ad hoc numerical models, the whole break up process, from the primary breakup to the secondary breakup, is reasonably investigated across the entire flow field. The penetration depth and spray cross-sectional distribution are compared with numerical and experimental data.

Keywords: *Homogeneous Mixture Model, Angled Liquid Jet in Supersonic Crossflow, Eulerian to Lagrangian, Adaptive Mesh Refinement*

Nomenclature

Latin
d – Diameter of injector
e – Specific internal energy
EtoL– Eulerian to Lagrangian
E_t – Specific total energy
h – Enthalpy
h_{fg} – Latent heat
$\dot{m}$ – Mass flow rate
MFR – Momentum flux ratio
N – Number of droplets
p – Pressure
q – Heat flux ratio
Q – Heat of reaction
S – Source term
t – Time
U_K – Reaction velocity of species k
T – Temperature
V – Volume
Y_k – Mass fraction of species k

Greek
γ – Ratio of specific heat
δ – Shock standoff distance
δ_{ij} – Kronecker delta
λ – Conductivity
μ – Viscous coefficient
ρ – Density
τ_{ij} – Viscous stress tensor

Superscripts
$\dot{}$ – Time difference

Subscripts
cri – Critical
d – Droplet
i, j, ij – Spatial coordinate index
L – Liquid phase

[1] *Korea Aerospace University, Goyang Gyeonggi 412-791 Republic of Korea, 010donggyu@kau.kr*
[2] *Korea Aerospace University, Goyang Gyeonggi 412-791 Republic of Korea, hgsung@kau.ac.kr*

1. Introduction

The utilization of a liquid jet in crossflow has been widely used in airbreathing engines such as gas turbine [1], ramjets [2], and scramjets [3,4]. The operation of scramjet engines depends on achieving optimal and efficient mixing of liquid fuel and supersonic crossflow, primarily due to the restricted residence time of the fuel in the combustor [5]. Thus, the combustion efficiency and thrust performance are greatly influenced by the mixture of fuel and air [6]. Methods to enhance atomization and mixing include momentum flux ratio, geometric design of orifices, aerated liquid jet, and angled injected liquid jet and so on. Among these, the angled injected liquid jet is particularly convenient to implement and requires no additional work [7]. Rodney et al. [8] analyzed the total pressure loss in Ma=5.0 crossflow with different incidence angles and total pressures. They explained that the total pressure loss decreased as both the incidence angle and injection pressure decreased. Wei [9] comprehensively investigated the interaction between injection angle and distance to the injectors on the flow characteristics of Ma=3.5 crossflow. They confirmed that the multi-port injection with a 30°injection angle provided a higher total pressure recovery efficiency than the single transverse injection method, with the total pressure recovery efficiency reaching 90%. Dixon [10] compared the penetration depth for injection angle of 90° or less using shadowgraph imagery. It was demonstrated that increasing the injection angle towards normal injection enhanced spray penetration, and based on experimental data, and derived the following correlation for liquid jets with respect to injection angle. Li et al. [11] found that variations in injection angle had a weak impact on penetration depth in a supersonic crossflow, while increasing injection angle resulted in larger shockwave angles and negatively affected total pressure recovery. Numerical simulations [12,13] provided detail insight into the flow structures around the liquid column and the distribution of droplets compared to experiments [14,15]. As such, there are few numerical studies conducted on injection angle, especially those exceeding 90°. In this study, the atomization process of a liquid dodecane jet in supersonic crossflow is investigated using the homogeneous mixture model which has only one type of governing equation for compressible multi-phase flow. In addition, the adaptive mesh refinement technique (AMR) and Eulerian to Lagrangian transformation (EtoL) are implemented for both efficient computational cost and detail liquid- breakup simulation. The vortices and flow patterns around the liquid column are observed. Bow shocks occurring ahead of the liquid column, as well as oblique shocks and expansion waves generated by the divergent channel, are identified. In addition, variations in penetration depth due to injection angle are compared with empirical and numerical results.

2. Numerical method

2.1. Governing equation

The three-dimensional unsteady Navier-Stokes equations, utilizing the homogeneous mixture model, are discretized using the finite volume method. The governing equations depict the conservations of mass, momentum, energy, and chemical species in Cartesian coordinates, as shown in Eq. (1) through Eq. (4). The indices *i* and *j* represent spatial coordinates, while *k* denotes the index for different species.

$$\frac{\partial \rho}{\partial t} + \frac{\partial \rho u_i}{\partial x_i} = \dot{S_c} \tag{1}$$

$$\frac{\partial \rho u_i}{\partial t} + \frac{\partial \rho u_i u_j}{\partial x_j} = -\frac{\partial p}{\partial x_i} + \frac{\partial \tau_{ij}}{\partial x_j} + \dot{S_M} \tag{2}$$

$$\frac{\partial \rho E}{\partial t} + \frac{\partial (\rho E_t + p) u_i}{\partial x_j} = -\frac{\partial q_j}{\partial x_j} + \frac{\partial u_i \tau_{ij}}{\partial x_j} + \dot{S_e} \tag{3}$$

$$\frac{\partial \rho Y_k}{\partial t} + \frac{\partial \rho u_j Y_k}{\partial x_j} = -\frac{\partial (\rho V_{ij} Y_k)}{\partial x_j} + \dot{S_{S,k}} \tag{4}$$

The viscous stress tensor (τ) and heat flux vector (q) for Newtonian fluid are defined as Eqs. (5) and (6), respectively. μ, λ, e, and h represent the viscosity coefficient, thermal conductivity, specific internal energy, and specific enthalpy, respectively.

$$\tau_{ij} = \mu\left(\frac{\partial u_i}{\partial x_j} + \frac{\partial u_j}{\partial x_i}\right) - \frac{2}{3}\mu\frac{\partial u_l}{\partial x_l}\delta_{ij} \tag{5}$$

$$q_j = -\lambda\frac{\partial T}{\partial x_j} + \rho\sum_{k=1}^{N} h_k Y_k U_{k,j} \tag{6}$$

A Lagrangian approach is employed to track the liquid droplet following secondary breakup. To couple the droplet with Eulerian field, the source term is conducted as shown in Eq. 7.

$$S = \begin{bmatrix} \dot{S}_c \\ \dot{S}_{M,i} \\ \dot{S}_E \\ \dot{S}_{s,k} \end{bmatrix} = \frac{1}{V}\begin{bmatrix} \dot{m}_p N_p \\ (\dot{m}_p u_{i,p} - \frac{4\pi}{3}\rho r^3\frac{\partial u_{i,p}}{\partial t})N_p \\ (\dot{m}_p h_{fs} + \dot{Q}_s)N_p \\ \dot{m}_{p,k} N_p \end{bmatrix} \tag{7}$$

2.2. Equation of state

The equation of state utilized is the Nobel-Abel Stiffened Gas (NASG) EOS [16], which applicable in the liquid phase. NASG EOS offers the advantage of encompassing both liquid and gas phases in a single equation and can be suitable over a relatively broad range of pressure and temperature. The pressure and internal energy derived from the NASG EOS are described by c_v , γ , b , p_∞ and Q, representing the heat capacity at constant volume, heat capacity ratio, co-volume, stiffness parameter, and heat bond, respectively. These parameters of constant coefficients that characterize the thermodynamic properties of the fluid. The term $(\gamma - 1)/(v - b)$ accounts for thermal agitation, where $(v - b)$ signifies the effect of strong repulsive short-range interactions between molecules associated with molecular motion in gases, liquids, and solids.

Table 1. The NASG EOS properties for the liquid water.

Liquid	γ	c_v(J/kg·K)	b (m³/kg)	p_∞(kPa)	Q (kJ/kg)
Water	1.19	3,610	6.721×10^{-4}	621,780	-1,177

2.3. Numerical schemes

In the multi-phase supersonic crossflow, it is crucial to maintain discontinuity while avoiding numerical oscillations in regions with large density gradients near the phase interface and strong shockwaves. To resolve the discontinuity without numerical oscillations, the Riemann solver in the model employs a combination of two techniques: the Harten-Lax-van Leer Contact with low dissipation (HLLCL) scheme [17] for the mass flux term and the simple low-dissipation AUSM2 (SLAU2) scheme [18] for the pressure flux term. Additionally, the viscous flux is computed using the central scheme. To prevent the numerical diffusion of liquid, the modified switching techniques for advection and capturing of surfaces (MSTACS) [19] is applied to the mass fraction. The van Leer limiter [20] is utilized for high-order reconstruction of remaining variables. Temporal discretization is achieved through a second-order backward differencing scheme [21]. Incorporating continuum surface force (CSF) is essential for modeling surface tension effects. Adaptive mesh refinement (AMR) techniques are implemented to observe detailed physical phenomena at the interface. During AMR application, a dynamic load balancing technique with a repartitioning method is used to address grid imbalances among processors. The finite volume method coupled with large eddy simulation using the wall-adapting local eddy-viscosity model (WALE) [22] is employed to account for the turbulent effects.

3. Model description

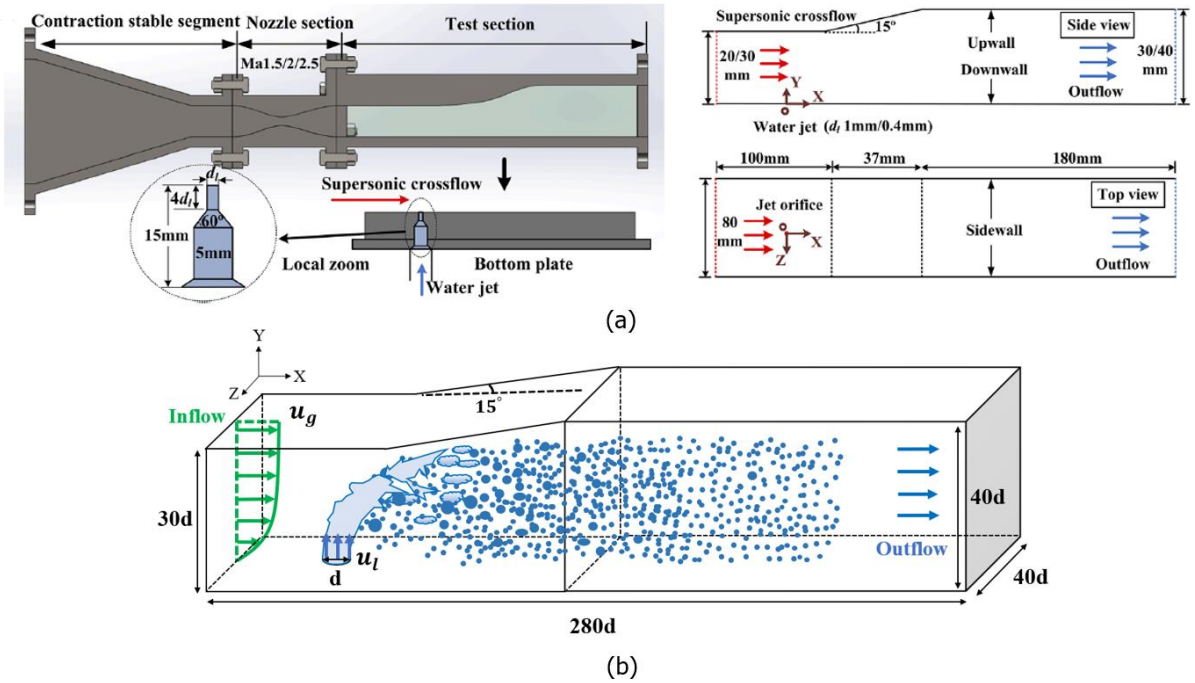

Fig 1. Schematic of wind tunnel experimental section (a) and computational domain (b).

The wind tunnel experimental setup is depicted in Fig. 1 (a), and the computational domain set around the injector is shown in Fig. 1 (b). The injector diameter (d) is 1 mm. The three-dimensional domain spans [0.0d, 280.0d]×[0.0d, 40.0d]×[0.0d, 40.0d] (length x width x height), with an expansion angle of 15°. The liquid injector is positioned 20d downstream from the inlet boundary. The minimum grid spacing is d/150, and the mesh comprises 4.6×10^{6} cells. For boundary conditions, supersonic inlet and outlet conditions are enforced, while no-slip wall condition is applied to the top and bottom. The inlet velocity profile utilizes experimental data representing fully developed flow. The Mach number of supersonic crossflow is 2.0. The pressure is 29 *kPa*, the temperature is 300 *K*, and the liquid is injected at angles of 60°, 90°, 120° with an MFR=8.0.

4. Results and discussion

Figs. 2(a) and (b) present the flow structures and shock waves in a rectangular channel with an expansion section using shadowgraph maps and magnetic images. Fig. 2 (c) observes the recirculation zone utilizing a schlieren picture [23]. Fig. 2(d) represents numerical results compared with experiments using density gradient magnitude contours. In front of the liquid column, a boundary layer leads to boundary separation, while behind the column, a strong recirculation flow is observed due to the interaction between the liquid jet and crossflow. This recirculation causes various vortices such as a horse-shoe vortex, wake vortex, and counter-rotating vortex pair (CVP). The velocity vector of the crossflow moving around the liquid column, changes direction downwards due to the density and pressure gradient, known as the liquid trailing phenomenon.

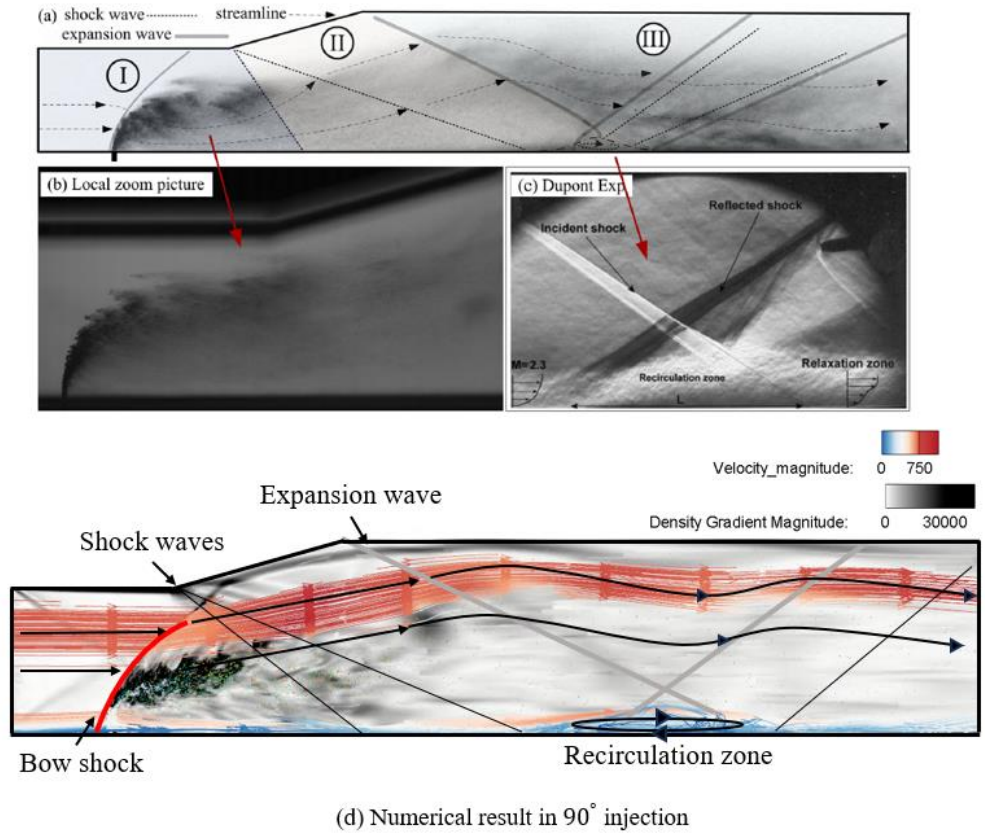

(d) Numerical result in 90° injection

Fig 2. Schematic diagram of wind tunnel experiments ((a)-(c)) and density gradient magnitude of numerical result (d).

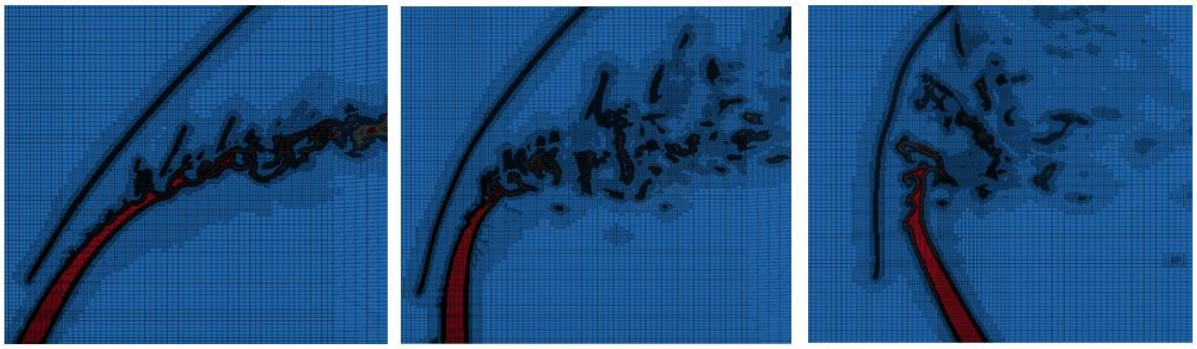

(a) 60° injection (b) 90° injection (c) 120° injection

Fig 3. Grid variation using AMR based on injection angle.

Fig. 3 illustrates the variations in the grid structure induced by AMR. Instead of maintaining a fine mesh throughout the entire domain, AMR directs computational resources to areas where they are most essential. Grid refinement occurs automatically in areas with significant variations in pressure and density. The minimum grid used in the domain before employing AMR is 150μm. Subsequently, the grid becomes denser near the shock waves and the liquid phase interface of the liquid column surface, showing a wavy surface due to surface instabilities and ligaments.

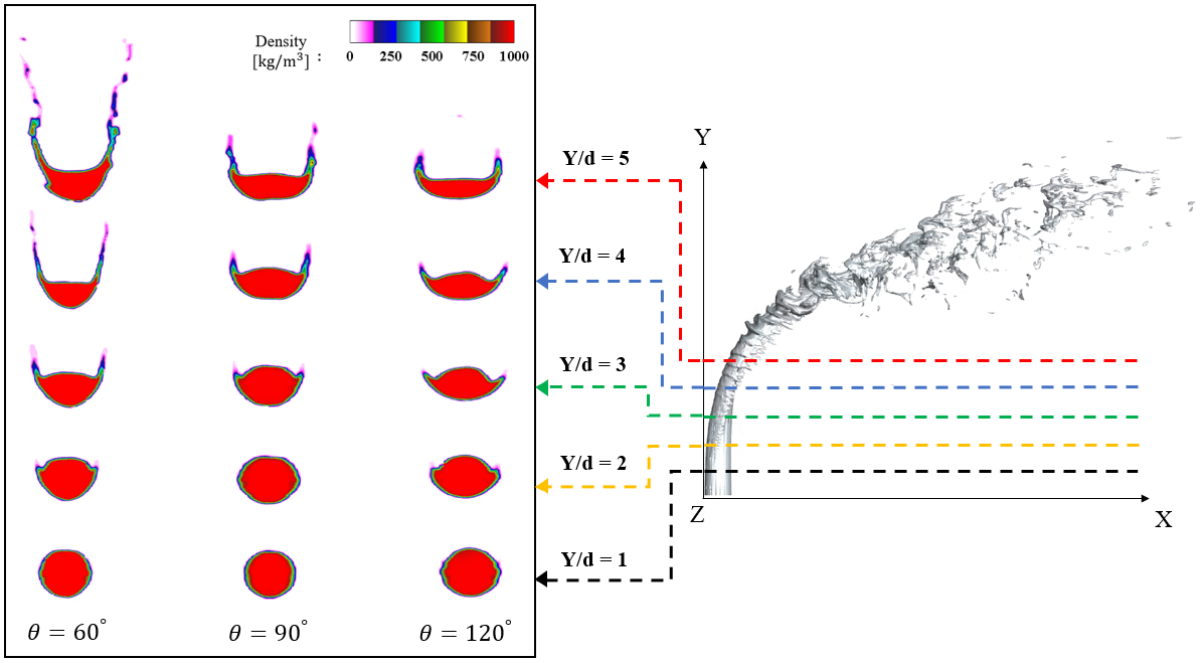

Fig 4. The variation of the liquid jet cross sectional area at *Y/d* = 1,2,3,4, and 5 for injection angles $\boldsymbol{\theta = 60^{\circ}, 90^{\circ}, \text{and } 120^{\circ}}$.

The liquid jet cross-section, depicted as density contours, is presented in Fig. 4 based on injection angle and liquid jet height. In all computed conditions, it is evident that the primary flow bends the liquid column. Intense shear forces cause liquid ligaments to detach as waves from both sides of the column. For the largest injection angle ($\boldsymbol{\theta = 120^{\circ}}$), ligaments separate the fastest, and the liquid column struggles to maintain continuity, quickly breaking up after leaving the liquid injector, which resulting in a flatter cross-sectional area of the liquid column and ligaments.

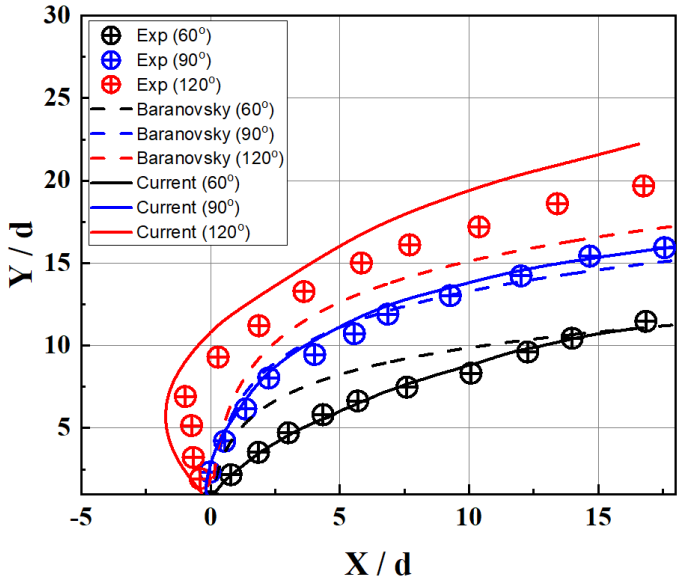

Fig 5. Comparison of penetration depth of experiment data, empirical formula, and current results.

The penetration depth obtained from an experiment data [23], Baranovsky formula [24], and the current numerical analysis are compared as shown in Fig. 5. Baranovsky formula is shown in Eq. (8).

The analysis results of water penetration depth are similar experimental data. The empirical formula matches at $\theta = 90^{\circ}$ but not consistently aligned at $60^{\circ}$and 120°.

$$Y/d = 1.32q^{0.5} ln\,[1 + 6\left(\frac{X}{d}\right)]sin\,(\frac{2\theta}{3}) \tag{8}$$

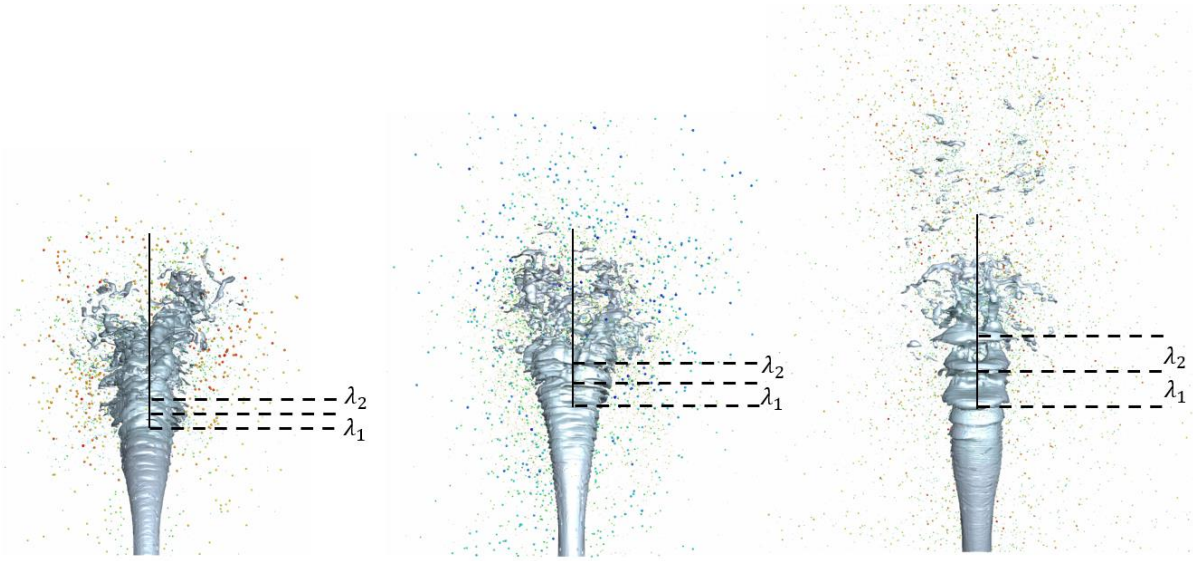

(a) $\theta = 60^{\circ}$ (b) $\theta = 90^{\circ}$ (c) $\theta = 120^{\circ}$

Fig 6. Primary and secondary breakup and liquid surface wavelength.

Due to the strong pressure difference between the upward and leeward sides of the liquid column, the gas flow significantly accelerates the liquid column, leading to the onset of Rayleigh-Taylor instability. Fig. 6 shows the wavelength of the liquid jet surface, which increases with the injection angle.

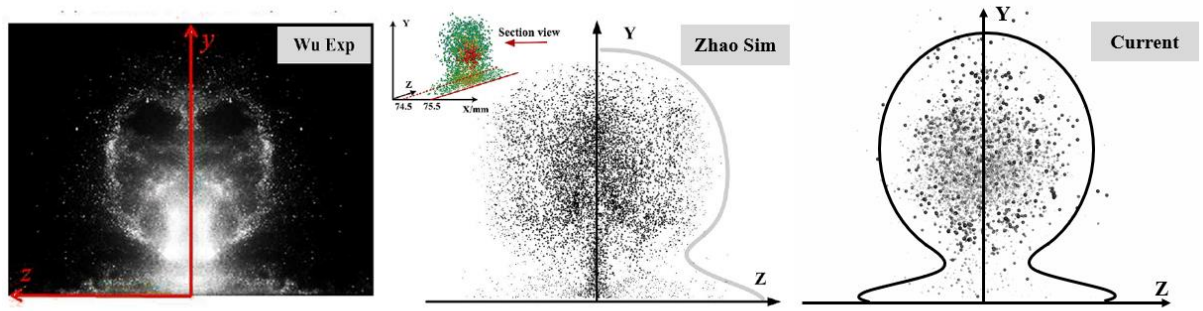

(a) Wu's experiment (b) Zhao's numerical result (c) Current result

Fig 7. Comparison of the spray shape on the cross-sectional plane (X=0.075 m) with experiment and numerical results.

Fig. 7 represents the distribution of sprays at the cross-section at X=0.075 m. Fig. 7 (a) displays the experimental image [25], utilizing the particle image velocity technique, while Fig. 7 (b) shows the numerical analysis results [26], using the TAB model. Fig. 7 (c) depicts the distribution of droplets after primary and secondary breakup in the current results. In all the cases, the spray distribution exhibits an omega shape, indicating a concentration of distribution around the liquid jet due to supersonic crossflow.

5. Conclusion

A compressible multi-phase large eddy simulation, inhouse code, is developed and conducted to investigate the breakup of the angled liquid water jet in supersonic crossflow of air with Mach number 2.0. The governing equations, which utilize the homogeneous mixture model, are expressed in general forms, and the equation of state is capable of simulating both gas and liquid phases. The NASA polynomial EOS is applied to the gas phases, and NASG EOS is applied to the liquid phases. The combination of convective flux HLLCL and SLAU2 is utilized, and MSTACS is applied to the mass fraction to prevent numerical diffusion. The surface tension force is calculated using a CSF model. To conduct a detailed analysis, AMR and EtoL transformation are implemented near the interface between the phases. As a result, the entire process of angled liquid water jet breakup from the liquid column is accurately simulated and validated. Kelvin-Helmholtz instability causes numerous liquid breakups into ligaments. Surface instability arising from the interaction between the liquid jet and supersonic crossflow, as well as complex shock waves and vortices, are observed, such as bow shock, separation shock, horse-shoe vortex, wake vortex, counter-rotating vortex pair, and liquid trailing phenomenon. The penetration depth according to injection angle is compared with experimental data and empirical formula from the 1st breakup through 2nd breakup region. The variation in liquid jet cross-sectional area, wavelength, and spray distributions according to injection angle is analyzed.

References

[1] Cavaliere, A., Ragucci, R., Noviello, C.: Bending and break-up of a liquid jet in a high pressure airflow. Experimental Thermal and Fluid Science. 27, 449-454 (2003)
[2] Inamura, T., Nagai, N.: Spray Characteristics of Liquid Jet Traversing Subsonic Airstreams. Journal of Propulsion and Power. 13, 250-256 (1997)
[3] Ren, Z., Wang, B., Xiang, G., Zhao, D., Zheng, L.: Supersonic spray combustion subject to scramjets: Progress and challenges. Progress in Aerospace Sciences. 105, 40-59 (2019)
[4] Sharma, V., Eswaran, V., Chakraborty, D.: Effect of fuel-jet injection angle variation on the overall performance of a SCRAMJET engine. Aerospace Science and Technology. 100, 105786 (2020)
[5] Hagen, W. A.: Numerical modeling of liquid jets in crossflow with applications to supersonic combustion ramjets. Thesis and Dissertations, Iowa State University, Ames, Iowa, USA (2017)
[6] Tian, Y., Yang, S., Le, J.: Study on flame stabilization of a hydrogen and kerosene fueled combustor. Aerospace Science and Technology. 59, 183-188 (2016)
[7] Zhou, W., Chen, B., Zhu, Q., Rao, S., Xu, X.: Numerical simulation of angled-injected liquid jet breakup in supersonic crossflow by a hybrid VOF-LPT method. International Journal of Multiphase Flow. 166, 104503 (2023)
[8] Rodeny, D. W., Fan, H., Lee, D.: Sonic Injection into a Mach 5.0 Freestream Through Diamond Orifices. Journal of Propulsion and Power. 20, 280-287 (2004)
[9] Huang, W.: Numerical investigation on staged sonic jet interaction mechanism in a supersonic crossflow. Journal of Aerospace Engineering. 228, 1-11 (2014)
[10] Dixon, D. R.: Structures of Angled-Aerated-Liquid Jets in Mach 1.94 Supersonic Crossflow. Thesis and Dissertations, Department of the Air Force Air University, Ohio, USA (2005)
[11] Li, C., Ma, L., Xia, Z., Chen, B., Feng, Y., Duan, Y.: Numerical investigation on mixing process of a sonic fuel jet into a supersonic crossflow. International Journal of Hydrogen Energy. 47, 37025-37039 (2022)
[12] Xiao, F., Wang, Z. G., Sun, M. B., Liang, J. H., Liu, N.: Large eddy simulation of liquid jet primary breakup in supersonic air crossflow. International Journal of Multiphase Flow. 87, 229-240 (2016)
[13] Zhao, J., Yan, C., Wu, L., Lin, W., Tong, Y., Nie, W.: Numerical simulation of singe/double liquid jets in supersonic crossflow. Aerospace Science and Technology. 120, 107289 (2022)
[14] Wu, L., Wang, Z. G., Li, Q., Zhang, J.: Investigations on the droplet distributions in the atomization of kerosene jets in supersonic crossflows. Applied Physics Letters. 107, 104103 (2015)
[15] Li, C., Li, P., Li, C., Li, Q., Zhou, Y.: Experimental and numerical investigation of cross-sectional structures of liquid jets in supersonic crossflow. Aerospace Science and Technology. 103, 105926 (2020)
[16] Metayer, O., Saurel, R.: The noble-abel stiffened-gas equation of state. Physics of Fluids. 28, 046102 (2016)

[17] Kitamura, K., Shima, Eiji.: AUSM-like expression of HLLC and its all-speed extension. International Journal Numerical Methods in Fluids. 92, 246-265 (2019)
[18] Kitamura, K., Shima, Eiji.: Pressure-equation-based SLAU2 for oscillation-free, supercritical flow simulations. Journal of Computers and Fluids. 163, 86-96 (2018)
[19] Van Leer, B.: Towards the ultimate conservative difference scheme II. Monotonicity and conservation combined in a second order scheme. Journal of Computational and Physics. 14, 361-370 (1974)
[20] Anghan, C., Bade, M. H.: A modified switching technique for advection and capturing of surfaces. Applied Mathematical Modeling. 92, 349-379 (2021)
[21] Hongfa, H.: Large-Eddy Simulation of Supercritical Fluid flow and Combustion. Thesis and Dissertations, Pennsylvania State University, USA (2011)
[22] Nicoud, F., Ducros, F.: Subgrid-Scale Stress Modelling Based on the Square of the Velocity Gradient Tensor. Turbulence and Combustion. 62, 183-200 (1999)
[23] Zhao, J., Tong, Y., Ren, Y., Zhu, Y., Chen, Z., Lin, W., Nie, W.: Structures of liquid jets in supersonic crossflows in a rectangular channel with an expansion section. Physics of Fluids. 32, 111704 (2020)
[24] Baranovsky, S. I., Schetz, J. A.: Effect of Injection Angle on Liquid Injection in Supersonic Flow. AIAA Journal. 18, 625-629 (1980)
[25] Wu, L. Y., Breakup and Atomization Mechanism of Liquid Jet in Supersonic Crossflows. Thesis and Dissertations. National University of Defense Technology, China (2016)
[26] Zhao, J., Ren, Y., Tong, Y., Lin, W., Nie, W.: Atomization of a liquid jet in supersonic crossflow in a combustion chamber with an expanded section. Acta Astronautica. 180, 35-45 (2021)